Direct numerical solution of the master-equation transport on disordered lattices via the Lanczos algorithm

Mark S. Friedrichs and Richard A. Friesner
Department of Chemistry, The University of Texas at Austin, Austin, Texas 78712
(Received 10 April 1987)

We investigate the diffusion problem on random networks in two dimensions by directly calculating matrix elements of transport operators on percolating clusters with up to 440 000 sites. The mean-square displacement, diffusion coefficient, and probability of returning to the origin are calculated and then analyzed in the context of dynamical scaling theory. From these results, we delineate the time and density regimes over which scaling arguments are quantitative. We also show the relative fluctuations in the random walk and present evidence that the eigenvalues and eigenvectors of the transfer rate matrix become Euclidean at different points in spectral space.

I. INTRODUCTION

The dynamics of many disordered condensed phase systems can be profitably modeled by random walks on networks generated by percolation processes. Examples include the transport of localized excitations in mixed organic crystals[1-3] and glasses,[4-5] and the conductivity of composites[6] and dispersed ionic conductors.[7] In these systems, transfer occurs via a short-ranged hopping mechanism so that percolative behavior may be seen.

A wide array of theoretical approaches have been developed in an effort to understand and characterize such systems: effective medium theories,[8-11] continuous-time random walks,[12-14] series expansions,[15-17] renormalization-group techniques,[18,19] and scaling arguments.[20-30] These methods have provided a qualitative and, in some cases, a quantitative description of the behavior of transport observables. For the most part, however, these approaches are strictly valid for only limited density or time regimes. For instance, in recent years scaling approaches in conjunction with fractal concepts have provided a detailed picture of transport near the percolation threshold, ρ_c. As shown here, however, this picture is quantitatively accurate only for either asymptotically long times or densities ρ such that $(\rho/\rho_c)-1<0.012$ $(\rho>\rho_c)$.

Monte Carlo experiments[20,31-41] have also shed considerable insight on transport in disordered systems, often complementing the above analytical techniques. For example, computer simulations have provided accurate estimates of critical exponents, and have confirmed and clarified the basic conclusions of scaling theory. A primary consideration in Monte Carlo studies of random walks is the computational effort required to collect sufficient statistics for the determination of a particular observable. This is especially important for walks on percolating systems due to the presence of both spatial and temporal fluctuations. Thus, averages must be performed over not only cluster configurations consistent with a specified density, but also over many walks on a given cluster. If the major contributions to an observable depend on a small percentage of the total number of possible walks, as in the case of the long-time behavior of $P_0(t)$, the probability of returning to the initial position at time t, then the computation cost may be prohibitive.

In this paper, we investigate diffusion on percolating networks by directly calculating matrix elements of transport operators for systems large enough to yield physically meaningful results. This strategy is made feasible by recent advances in numerical analysis and the development of the recursive residue generation method by Wyatt and co-workers.[42] The main advantages of this approach are the following.

(1) It can provide quantitative results for any time or density regime.

(2) The temporal statistics are exact, and hence only configurational averages and, in some cases, averages over starting positions are required.

(3) The method is sufficiently general to handle not only the canonical percolation transport problem, but also related problems involving traps,[43-45] anisotropic diffusion,[46-49] non-nearest-neighbor transfer,[50] and polymers.[51,52]

We have used the procedure here to determine $P_0(t)$, $R^2(t)$ (the mean-square displacement of the walker at time t), and $D(t)$ (the associated diffusion coefficient) for the site percolation problem on the two-dimensional square lattice with diffusion governed by the Pauli master equation. In Secs. II and III, the methods are discussed in detail. The results of calculations on the percolating cluster for densities in the range $\rho=0.60-0.70$ are presented in Sec. IV and then analyzed in the framework of dynamical scaling theory. We also show the variance of $R^2(t)$, and present evidence suggesting that the density of states and eigenvectors of the transition rate matrix become Euclidean-like at different points in the spectrum of the matrix. In Sec. V, we summarize our results and compare the relative merits of Monte Carlo simulations to the algorithms discussed here.

II. $P_0(t)$

The specific model considered is site percolation on the two-dimensional square lattice. For an isolated cluster of open sites, the transport properties are assumed to

be governed by the Pauli master equation

$$\frac{dp_n(t)}{dt}=\sum_{m=1}^{N} w_{mn}p_m(t)-w_{nm}p_n(t), \quad n=1,\ldots,N \ . \tag{1}$$

Here $p_n(t)$ is the probability that site n is occupied by the walker at time t, w_{mn} is the transfer rate from site m to site n, and N is the number of open sites comprising the cluster. Eq. (1) may be rewritten in matrix form as

$$\frac{d\mathbf{P}(t)}{dt}=\underline{W}\mathbf{P}(t) \ , \tag{2}$$

where the nth element of the vector $\mathbf{P}(t)$ is $p_n(t)$, and the transfer rate matrix $\underline{W}$ is the $N\times N$ array consisting of the elements

$$[\underline{W}]_{mn}=(1-\delta_{mn})w_{mn}-\delta_{mn}\sum_{j=1}^{N} w_{nj} \ , \tag{3}$$

with δ_{mn} the Kronecker delta. The formal solution of Eqs. (1) and (2) is

$$\mathbf{P}(t)=e^{\underline{W}t}\mathbf{P}(t=0)=\underline{G}(t)\mathbf{P}(t=0) \ , \tag{4}$$

where $\mathbf{P}(t=0)$ is the initial probability distribution of occupied sites. The matrix elements of the Green's function $\underline{G}(t)$, $G_{mn}(t)=\langle m \mid \underline{G}(t) \mid n \rangle$, give the conditional probability that site m is occupied at time t, if site n is occupied at $t=0$.

In particular, the diagonal elements of $\underline{G}(t)$ give the probability the walker returns to its original position. Therefore, assuming a uniform initial probability distribution of occupied sites [that is, $p_n(t=0)=(1/N)$ for all n], $P_0(t)$ is given by the expression

$$P_0(t)=\frac{1}{N}\sum_{j=1}^{N}\langle j \mid \underline{G}(t) \mid j \rangle=\frac{1}{N}\mathrm{Tr}[\underline{G}(t)]=\frac{1}{N}\mathrm{Tr}(e^{\underline{W}t}) \ . \tag{5}$$

Recalling that the trace of a matrix is equal to the sum of its eigenvalues,

$$P_0(t)=\frac{1}{N}\sum_{j=1}^{N} e^{\lambda_j t} \ , \tag{6}$$

where $\{\lambda_j\}_{j=1}^{N}$ is the spectrum of the transfer rate matrix $\underline{W}$. The problem of calculating $P_0(t)$ is thereby reduced to determining the density of states of $\underline{W}$.

The eigenvalues of $\underline{W}$ are found by first using the Lanczos algorithm, as modified by Paige[53,54] and Cullum and Willoughby,[55] to generate a symmetric, tridiagonal matrix $\underline{T}$ which is related to $\underline{W}$ by a similarity transformation; the bisection method[56] is then employed to determine $\underline{T}$'s spectrum. Briefly, the Lanczos algorithm tridiagonalizes $\underline{W}$ by constructing a sequence of orthonormal vectors $\{\mathbf{v}_i\}$ from an initial vector $\mathbf{v}_1$ according to the recursion formula

$$\beta_{j+1}\mathbf{v}_{j+1}=\underline{W}\mathbf{v}_j-\alpha_j\mathbf{v}_j-\beta_j\mathbf{v}_{j-1}, \quad j=1,\ldots,m \tag{7}$$

with

$$\alpha_j=(\underline{W}\mathbf{v}_j,\mathbf{v}_j) \ ,$$

$$\beta_{j+1}=\|\underline{W}\mathbf{v}_j-\alpha_j\mathbf{v}_j-\beta_j\mathbf{v}_{j-1}\| \ ,$$

$\mathbf{v}_0=\mathbf{0}$ and $\beta_1=0$. The α_j and β_j form, respectively, the diagonal and off-diagonal of the $m\times m$ matrix $\underline{T}$. The procedure is well-suited for the present problem since the storage requirements are between $6N$ and $8N$: $3N$ for the Lanczos vectors $\mathbf{v}_i$, $1N-2N$ for $\underline{T}$ as explained below, and by structuring the sparsity, approximately $2N-3N$ for performing the matrix multiplication $\underline{W}\mathbf{v}_j$, depending on the density; thus clusters on the order of 10^5 sites may easily be handled on a Cray X-MP or Cyber 205 supercomputer. Moreover, by exploiting the sparsity of $\underline{W}$, the number of arithmetic operations required by the Lanczos procedure is $O(N^2)$, in contrast to other tridiagonalization routines which cannot take full advantage of $\underline{W}$'s sparsity and therefore typically scale as N^3.

In exact arithmetic, the Lanczos algorithm would terminate at the mth recursion ($\beta_{m+1}=0$, $m\leq N$) with the m eigenvalues of $\underline{T}$ corresponding to the m distinct eigenvalues of $\underline{W}$ whose eigenvectors have a nonzero projection on $\mathbf{v}_1$. The use of finite-precision arithmetic, however, introduces roundoff error which in turn leads to a loss in the global orthogonality of the $\{\mathbf{v}_j\}_{j=1}^{m}$. This numerical instability has two important consequences. First, the requisite number of Lanczos steps is no longer bounded by N, but depends on the structure of $\underline{W}$'s spectrum and the location of the desired eigenvalues within the spectrum. Numerical experiments by Cullum and Willoughby[55] show that well-separated, extremal eigenvalues typically require the fewest number of recursions with $m\lesssim N$, whereas clustered eigenvalues in the interior of the spectrum may require m to be as large as $10N$. These general observations were found to hold here. If the time is scaled so that the transfer rate between any two open, nearest neighbors is 1 ($w_{mn}=1$), then the spectrum of $\underline{W}$ by Gerschgorin's theorem lies in the closed interval $[-8,0]$. For intermediate to long times ($t\gtrsim 100$), only eigenvalues in the range $[-0.1,0.0]$ make a significant contribution to the sum in Eq. (6). By systematically varying the number of Lanczos recursions for several fixed clusters, it was found that $m=0.7N$ to $0.8N$ was sufficient to secure the convergence of most of these eigenvalues for a random initial Lanczos vector, $\mathbf{v}_1$. By choosing $\mathbf{v}_1$ to be the sum of the low-**k** eigenvectors for the corresponding problem on the regular square lattice, we were able to reduce m to between 50–60 % of N. These observations are corroborated by Fig. 1, which shows the variation of $P_0(t)$ with the number of recursions for a cluster of $N=57\,500$ sites (density of 0.66 on a lattice of linear dimension 300) using a low-**k** eigenvector of the full lattice as an initial Lanczos vector. As seen in the figure, the results for recursion numbers greater than $0.5N$ essentially agree for all times greater than $t=100$, whereas for $m=0.32N$, the calculated $P_0(t)$ does not agree with the higher recursion numbers until times greater than 600.

A second manifestation of the Lanczos numerical instability is the breakdown of the isomorphism between the spectra of $\underline{T}$ and $\underline{W}$ which is present in exact arithmetic. There are two distinct aspects associated with

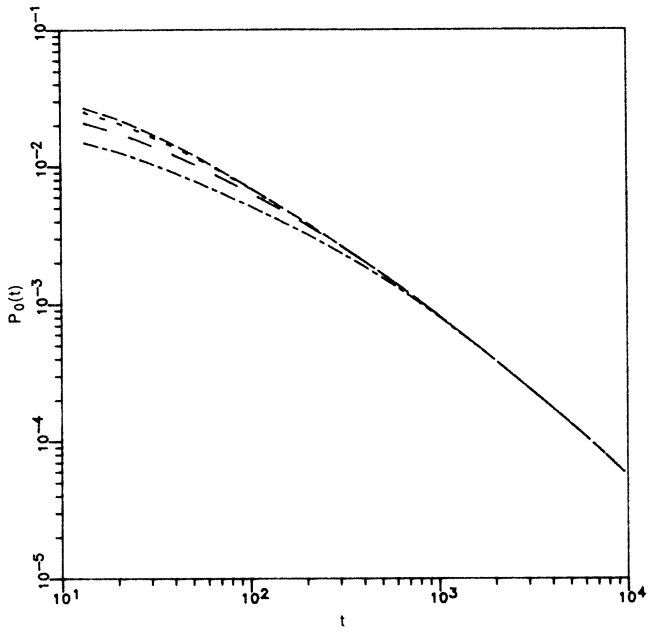

FIG. 1. Double-logarithmic graphs of $P_0(t)$ on a sample cluster of $N=57\,500$ sites (density of 0.66, linear dimension of lattice of 300) for a range of recursion numbers. From top to bottom, the curves correspond to the recursion numbers $m=0.8N$, $0.64N$, $0.48N$, and $0.32N$.

this breakdown: (1) the multiplicities of the eigenvalues of $\underline{T}$, in general, are not in accord with the eigenvalue multiplicities of $\underline{W}$, and (2) some eigenvalues of $\underline{T}$ are spurious, i.e., they are not eigenvalues of $\underline{W}$. This problem is easily circumvented by applying the following empirically based rules: (1) multiple eigenvalues of $\underline{T}$ are always eigenvalues of $\underline{W}$, and (2) nondegenerate eigenvalues of $\underline{T}$ are eigenvalues of $\underline{W}$ only if they are not eigenvalues of $\underline{T}'$, the tridiagonal matrix obtained by deleting the first row and column of $\underline{T}$. Thus, spurious eigenvalues are identified by their presence in both the spectrum of $\underline{T}$ and $\underline{T}'$.

Although no rigorous proof exists which validates these rules, they have been shown to be reliable for a variety of matrices.[55] We should stress that this procedure for extracting the eigenvalues of $\underline{W}$ from $\underline{T}$ is only feasible if the spectrum of $\underline{W}$ is known to be nondegenerate or the multiplicities of $\underline{W}$'s eigenvalues are not needed. For the current $\underline{W}$, diagonalizations using algorithms which yield the correct eigenvalue multiplicity show that for densities less than one, $\underline{W}$ is degenerate only for integer eigenvalues less than zero. Since these eigenvalues lie outside the relevant portion of the spectrum, the method as described is applicable.

As mentioned above, the eigenvalues of $\underline{T}$ are found using the bisection method. For the present problem, this algorithm possesses three important advantages over other algorithms for tridiagonal matrices, such as the rational QR transformation. First, it is straightforward to vectorize the Sturm-sequencing portion of the algorithm which dominates the central processing unit (CPU) time. Second, only the required eigenvalues are calculated, and these may be determined to a specified error tolerance. This is an important feature since, as pointed out earlier, the sum in Eq. (6) depends only on the distribution of eigenvalues near the front of the spectrum for the time scales of interest here. Finally, the spurious eigenvalues of $\underline{T}$ may be identified by one application of the Sturm-sequencing procedure to $\underline{T}'$, thereby eliminating the need to diagonalize $\underline{T}'$. These advantages taken together lead to dramatic reductions in the times required to diagonalize $\underline{T}$. Indeed, prior to our adoption of the bisection method, this part of the program completely dominated the computational time.

III. $R^2(t)$

In addition to $P_0(t)$, $R^2(t)$, and $D(t)$ were also calculated for the two-dimensional site percolation problem. Using the nomenclature established in Sec. II, $R^2(t)$ for an isolated cluster of N open sites is

$$\langle R^2(t)\rangle=\frac{1}{N}\mathrm{Tr}(\underline{R}^2e^{\underline{W}t})=\frac{1}{N}\sum_{j=1}^{N}\langle j\,|\,\underline{R}^2e^{\underline{W}t}\,|\,j\rangle\ , \tag{8}$$

where the (k,l) element of the $N\times N$ matrix $\underline{R}^2$ is the squared distance between sites k and l, and the $\{|\,j\,\rangle\}_{j=1}^{N}$ are the basis vectors in the site representation. Inserting a complete set of site states,

$$\begin{aligned}\langle R^2(t)\rangle&=\frac{1}{N}\sum_j\sum_i\langle j\,|\,\underline{R}^2\,|\,i\,\rangle\langle i\,|\,e^{\underline{W}t}\,|\,j\,\rangle\\&=\frac{1}{N}\sum_j\sum_i(\underline{R}^2)_{ij}\langle i\,|\,e^{\underline{W}t}\,|\,j\,\rangle\\&=\frac{1}{N}\sum_j\langle k_j\,|\,e^{\underline{W}t}\,|\,j\,\rangle\\&=\frac{1}{N}\sum_j R_j^2(t)\end{aligned} \tag{9}$$

with $|\,k_j\,\rangle=\sum_i|\,i\,\rangle(\underline{R}^2)_{ij}$. The matrix element $\langle k_j\,|\,e^{\underline{W}t}\,|\,j\,\rangle=R_j^2(t)$ represents the mean-square displacement of a walker at time t with its initial position at site j.

These matrix elements are determined by utilizing the recursive residue generation method (RRGM) developed by Wyatt and co-workers.[42] Following the presentation in Ref. 42,

$$\langle k_j\,|\,e^{\underline{W}t}\,|\,j\,\rangle=\sum_{\alpha=1}^{N}\langle k_j\,|\,\alpha\,\rangle\langle\alpha\,|\,j\,\rangle e^{\lambda_\alpha t} \tag{10}$$

where λ_α, and $|\,\alpha\,\rangle$ are the αth eigenvalue and eigenvector of $\underline{W}$, respectively. The important advantage offered by the RRGM is that the product of the projections of the eigenvectors onto $|\,k_j\,\rangle$ and $|\,j\,\rangle$ can be determined without resorting to an explicit calculation of the eigenvectors. Let

$$\begin{aligned}|\,u\,\rangle&=\frac{1}{\sqrt{2}}(|\,k_j\,\rangle+|\,j\,\rangle)\ ,\\|\,v\,\rangle&=\frac{1}{\sqrt{2}}(|\,k_j\,\rangle-|\,j\,\rangle)\ .\end{aligned} \tag{11}$$

The residue $\langle k_j\,|\,\alpha\,\rangle\langle\alpha\,|\,j\,\rangle$ is then seen to be

$$\langle k_j\,|\,\alpha\,\rangle\langle\alpha\,|\,j\,\rangle=\tfrac{1}{2}(\langle u\,|\,\alpha\,\rangle^2-\langle v\,|\,\alpha\,\rangle^2)\ . \tag{12}$$

The quantities $\langle u \mid \alpha \rangle^2$ (the calculation of the $\langle v \mid \alpha \rangle^2$ proceeds along similar lines) are the residues of the diagonal Green's function

$$G_u(z)=\langle u \mid (z\underline{I}-\underline{W})^{-1} \mid u \rangle = \sum_{\alpha} \frac{\langle u \mid \alpha \rangle^2}{z-\lambda_\alpha} \tag{13}$$

with the spectrum of $\underline{W}$ excluded from the domain of G_u. In a representation in which $\mid u \rangle$ is the first basis vector, Cramer's rule gives

$$\langle u \mid (z\underline{I}-\underline{W})^{-1} \mid u \rangle = \frac{\det(z\underline{I}-\underline{W})^D}{\det(z\underline{I}-\underline{W})} , \tag{14}$$

where $(z\underline{I}-\underline{W})^D$ is the matrix obtained by deleting the first row and column of $(z\underline{I}-\underline{W})$. Finally, using the relation

$$\det(z\underline{I}-\underline{W})=\prod_{\alpha=1}^{N}(z-\lambda_\alpha) ,$$

the residue

$$\begin{aligned}\langle u \mid \alpha \rangle^2 &= \lim_{z\to\lambda_\alpha}(z-\lambda_\alpha)G_u(z) \\ &= \lim_{z\to\lambda_\alpha}(z-\lambda_\alpha)\frac{\det(z\underline{I}-\underline{W})^D}{\det(z\underline{I}-\underline{W})} \\ &= \prod_{\beta=1}^{N-1}(\lambda_\alpha-\lambda_\beta^u)\Big/\prod_{\substack{\gamma=1\\ \gamma\neq\alpha}}^{N}(\lambda_\alpha-\lambda_\gamma)\end{aligned} \tag{15}$$

where $\{\lambda_\beta^u\}_{\beta=1}^{N-1}$ are the eigenvalues of $\underline{W}^D$.

Thus, in lieu of calculating the eigenvectors, $\mid \alpha \rangle$, the three sets of eigenvalues $\{\lambda_\alpha\}_{\alpha=1}^{N}$, $\{\lambda_\beta^u\}_{\beta=1}^{N-1}$, and $\{\lambda_\beta^v\}_{\beta=1}^{N-1}$ are used to determine the matrix element $\langle k_j \mid e^{\underline{W}t} \mid j \rangle$. These three sets are generated in two separate, modified implementations of the procedure sketched in Sec. II. In the first, the tridiagonal matrix $\underline{T}_u$ is constructed with a starting vector $\mathbf{v}_1=\mid u \rangle=(1/\sqrt{2})\{\mid k_j \rangle+\mid j \rangle\}$, and in the second $\mathbf{v}_1=\mid v \rangle=(1/\sqrt{2})\{\mid k_j \rangle-\mid j \rangle\}$ is used to generate $\underline{T}_v$. The dimension m of $\underline{T}_u$ and $\underline{T}_v$, i.e., the number of required iterations, is 1–5 % of N for the systems considered here. The relatively small size of m compared to N reflects the rapid convergence of the subspace spanned by the Lanczos vectors $\mathbf{v}_i$ to the subspace spanned by the eigenvectors which are strongly coupled to $\mid u \rangle$ and $\mid v \rangle$. Thus, most of the physics of $\underline{W}$ at intermediate to long times is confined to a small subspace of the full space spanned by $\underline{W}$, and the Lanczos method is able to home in on this subspace.

After $\underline{T}_u$ and $\underline{T}_v$ are generated, they and $\underline{T}_u'$ and $\underline{T}_v'$, the matrices obtained by deleting the first row and column of $\underline{T}_u$ and $\underline{T}_v$, are diagonalized using the bisection method. Because the product $\langle k_j \mid \alpha \rangle\langle \alpha \mid j \rangle$ is calculated as the difference of two residues [Eq. (12)], the accuracy to which these residues, and hence eigenvalues, are required is significantly higher (relative tolerance of 10^{-9}) than that needed for $P_0(t)$ or observables dependent on a single Green's function matrix element (relative tolerance of 10^{-7}), particularly for very large systems. Also, in contrast to the calculation of $P_0(t)$, the full spectra of the four matrices are needed, since the residues depend on the global distribution of the eigenvalues [Eq. (15)]. This is not a serious drawback, however, due to the small size of m.

The numerical instabilities associated with the Lanczos procedure are, of course, still present. Since the eigenvalues of both $\underline{T}_u$ and $\underline{T}_u'$ are available here, the removal of the spurious and multiple eigenvalues is accomplished by applying a linear algebra theorem which states that the spectra of $\underline{T}_u$ and $\underline{T}_v'$ must form a Sturm sequence, i.e., $\lambda_n<\lambda_n'<\lambda_{n+1}<\lambda_{n+1}'<\cdots$. Using this constraint, if $\mid(\lambda_n-\lambda_{n+1}')/\lambda_n \mid <\delta$ where δ is a specified error tolerance, then λ_n and λ_{n+1}' are both spurious and are deleted from their respective spectra. In practice it was found that the spectra were fairly insensitive to the precise choice of δ. Thus identical results were obtained for values of δ ranging from 5 to 100 times the relative tolerance to which the eigenvalues were obtained; in practice we took δ to be 10 times the eigenvalue tolerance. Once the four sets of eigenvalues have been purged of the unwanted eigenvalues, the residues [Eq. (15)] are calculated, and Eq. (10) is evaluated.

The diffusion coefficient, defined here to be $D(t)=[\partial R^2(t)/\partial t]$, is calculated by taking the time derivative of Eq. (10),

$$D_j(t)=\sum_{\alpha}\lambda_\alpha\langle k_j \mid \alpha \rangle\langle \alpha \mid j \rangle e^{\lambda_\alpha t} . \tag{16}$$

Thus, $D_j(t)$ is easily evaluated using the quantities from which $R_j^2(t)$ was calculated.

IV. RESULTS

$P_0(t)$, $R^2(t)$, and $D(t)$ were evaluated for the percolating cluster on lattices of linear dimension $L=300$ and 500, and in the cases of $R^2(t)$ and $D(t)$ at $L=800$, for concentrations in the interval [0.60,0.70]. At these densities, the clusters ranged in size from $N=40\,000$–$60\,000$ for $L=300$, to $N=300\,000$–$440\,000$ for $L=800$. In order to minimize finite-size effects, periodic boundary conditions were imposed; the metric in the calculation of $R^2(t)$ and $D(t)$ was taken to be the minimum distance between two sites in the resulting toroidal topology. At each density, the observables were averaged over different cluster configurations and, for $R^2(t)$ and $D(t)$, over different initial positions for a given cluster. By comparing two independent sets of calculations, we estimated that approximately 10 and 4 cluster configurations were required to secure convergence in determining $P_0(t)$ for $L=300$ and 500, where convergence is arbitrarily defined here and below to be a relative difference less than 5% between the two sets. For $R^2(t)$, 15 clusters with two initial points per cluster at $L=300$, 8 clusters with two starting points for each cluster at $L=500$, and at $L=800$, 8 clusters with only one initial site per cluster were needed to obtain agreement between two sets of calculations. At $\rho=0.60$ and $\rho=0.62$, the number of required configurations was significantly higher than those stated above (up to 15 clusters at $L=800$) due to the presence of relatively large spatial fluctuations in the clusters. The calculations for $P_0(t)$ at $L=300$ were made on a Cyber 205 and took approximately 1000 CPU sec, per cluster. The remaining calculations were

performed on a Cray X-MP; the evaluation of $P_0(t)$ required 3600 CPU sec per cluster, and for $R^2(t)$ at $L=800$, 600–1400 CPU sec per starting point were needed, depending on the density.

In Fig. 2, the graphs of $\ln P_0(t)$ versus $\ln t$ for the densities $\rho=0.68$, 0.66, and 0.64 at $L=500$ and $\rho=0.60$ at $L=300$ are shown. Figures 3 and 4 are plots of $R^2(t)$ and $D(t)$, respectively, at $L=800$ for six evenly spaced densities ranging from $\rho=0.60$–0.70. In the remainder of this section, the results for $R^2(t)$ and $P_0(t)$ are analyzed in the context of scaling theory. For both observables, estimates are made of the following quantities: (1) the effective time exponent as a function of time, (2) the scaling exponent associated with the diffusion coefficient in the Euclidean regime, and (3) the appropriate scaling function.

According to scaling arguments, the dependence of P_0 on t and ρ for walks restricted to the percolating cluster is given by[24]

$$P_0(t,\rho)\sim(t/\tau)^{-d/2}(\rho-\rho_c)^{dv-\beta}f_1(t/\tau)\ , \tag{17}$$

where d is the Euclidean dimension, $\tau\sim(\rho-\rho_c)^{-(2v-\beta+\mu)}$ is the mean time taken to diffuse the correlation length $\xi\sim(\rho-\rho_c)^{-v}$, β is the percolation probability exponent, μ is the conductivity exponent, and ρ_c is the critical density. For $d=2$, the expression reduces to

$$P_0(t,\rho)\sim t^{-1}(\rho-\rho_c)^{-\mu}f_1(t/\tau)\ . \tag{18}$$

The functional form of $f_1(x)$ is particularly simple in the limits $x\ll 1$ and $x\gg 1$:

$$f_1(x)\sim\begin{cases}x^{\mu/(2v-\beta+\mu)} & \text{for } x\ll 1\\ \text{const} & \text{for } x\gg 1\ .\end{cases} \tag{19}$$

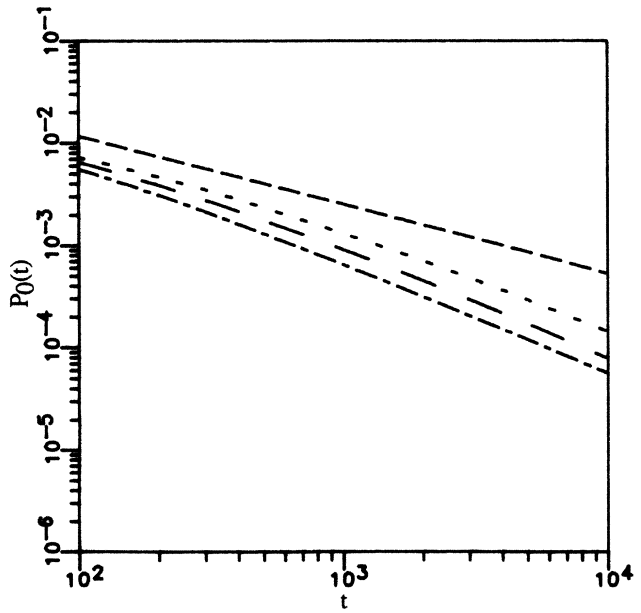

FIG. 2. Plot of $\ln P_0(t)$ vs $\ln t$ for four densities. From top to bottom, $\rho=0.60$ for a lattice of length $L=300$, and $\rho=0.64$, 0.66, and 0.68 at $L=500$.

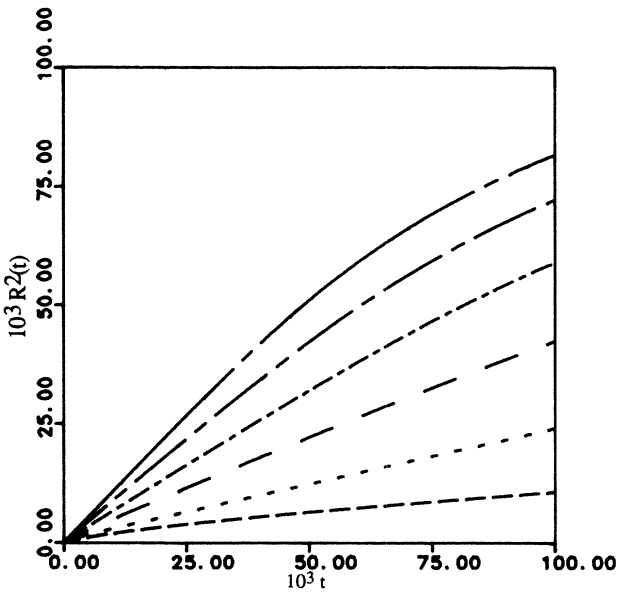

FIG. 3. $R^2(t)$ vs t for six densities on a lattice of length $L=800$. From top to bottom $\rho=0.70$, 0.68, 0.66, 0.64, 0.62, and 0.60.

Therefore, for times such that $1\ll t\ll\tau$ or, equivalently, on length scales $a^2\ll R^2(t)\ll\xi^2$ with a the lattice spacing,

$$P_0(t,\rho)\sim t^{-d_s/2}\ , \tag{20}$$

where d_s is the spectral dimension, $d_s=2(2v-\beta)/(2v-\beta+\mu)$. At long times $t\gg\tau$ or $R^2(t)\gg\xi^2$,

$$P_0(t,\rho)\sim(\rho-\rho_c)^{-\mu}t^{-1}=[D_1(\rho)t]^{-1} \tag{21}$$

with $D_1(\rho)\sim(\rho-\rho_c)^{\mu}$ the diffusion coefficient of P_0.

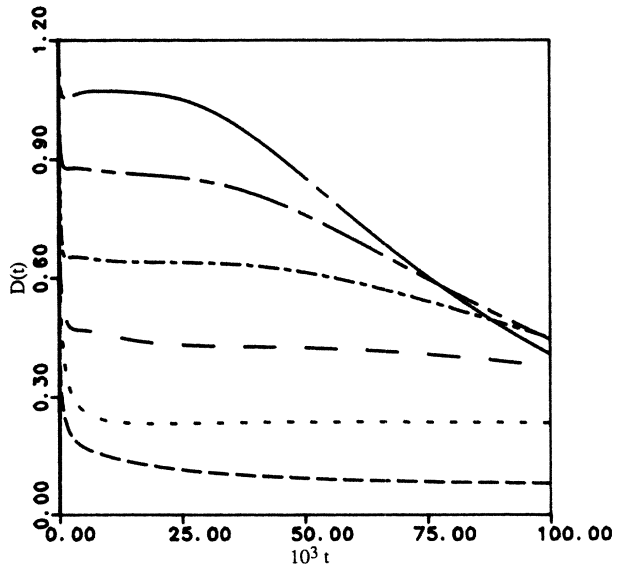

FIG. 4. Plot of $D(t)=\partial R^2(t)/\partial t$ for six densities on a lattice of length $L=800$. From top to bottom $\rho=0.70$, 0.68, 0.66, 0.64, 0.62, and 0.60.

The arguments used to derive the above asymptotic forms are based on the observation that for length scales less than ξ, the percolating cluster is statistically self-similar, whereas for length scales much greater than ξ, the percolating cluster is homogeneous. As a consequence, the random-walk observables undergo a crossover from behavior characteristic of transport on fractal lattices to behavior typical of regular lattices, i.e., the Euclidean regime.

The functional dependence of R^2 on t and ρ is, again from scaling arguments,[20]

$$R^2(t,\rho)\sim t^{2v/(2v-\beta+\mu)} f_2[(\rho-\rho_c)t^{1/(2v-\beta+\mu)}] , \quad (22)$$

where

$$\lim_{x\to 0} f_2(x)\sim \text{const} \quad (23)$$

and

$$\lim_{x\to\infty} f_2(x)\sim x^{\mu-\beta} .$$

Consequently, in the fractal regime $a^2 \ll R^2(t) \ll \xi^2$,

$$R^2(t,\rho)\sim t^{2v/(2v-\beta+\mu)} = t^{d_s/d_F} , \quad (24)$$

where d_F is the Hausdorff or fractal dimension, $d_F = d - (\beta/v)$. In the Euclidean limit $R^2(t) \gg \xi^2$,

$$R^2(t,\rho)\sim(\rho-\rho_c)^{\mu-\beta} t = D_2(\rho)t \quad (25)$$

with $D_2(\rho)$ the diffusion coefficient of R^2.

Figures 5 and 6 show the effective time exponents $\alpha_1(t)$ and $\alpha_2(t)$ of $P_0(t)$ and $R^2(t)$, respectively, where

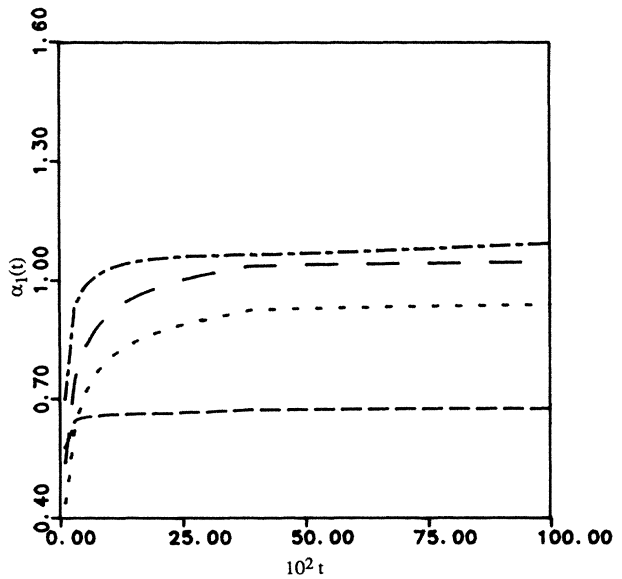

FIG. 5. Graph of the effective time exponent of $P_0(t), \alpha_1(t)$, where $P_0(t)\sim t^{-\alpha_1(t)}$. α_1 at t was found by performing a linear least-squares fit to the curve $\ln P_0(t)$ vs $\ln t$ for time grid points in the immediate neighborhood of t; the slope of the resulting line was taken to be $\alpha_1(t)$. The upper three curves were derived from calculations on a lattice of length $L=500$ at the concentrations $\rho=0.68$ (——·——), $\rho=0.66$ (— — —), and $\rho=0.64$ (---), and the lower curve from calculations on lattices with $L=300$ and $\rho=0.60$ (– – –).

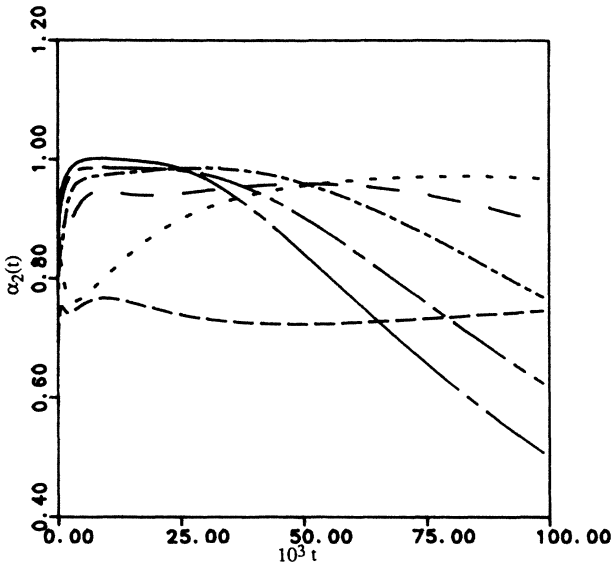

FIG. 6. Plots of the effective time exponent of $R^2(t), \alpha_2(t)$, where $R^2(t)\sim t^{\alpha_2(t)}$ on lattices of length $L=800$. α_2 at time t was estimated by performing a linear least squares fit to the graphs $\ln R^2(t)$ vs $\ln t$ for time points near t; the slope of the resulting line was taken to be $\alpha_2(t)$. The six densities shown are $\rho=0.70$ (——-), $\rho=0.68$ (——·——), $\rho=0.66$ (—·—), $\rho=0.64$ (— —), $\rho=0.62$ (---), and $\rho=0.60$ (– – –).

$P_0(t)\sim t^{-\alpha_1(t)}$ and $R^2(t)\sim t^{\alpha_2(t)}$. These functions were obtained by performing a linear least-squares fit to the graphs of $\ln P_0(t)$ versus $\ln t$, and $\ln R^2(t)$ versus $\ln t$ for time points in the immediate neighborhood of t; the slope of the resulting line was taken to be the value of α_1 or α_2 at time t.

At $\rho=0.60$, the correlation length is relatively large so that on the time scales over which the calculations were made, the transport observables should exhibit the anomalous behavior characteristic of the fractal regime. Hence, $P_0(t)$ should vary as $P_0(t)\sim t^{-0.66}$, and $R^2(t)$ as $R^2(t)\sim t^{0.70}$. The numbers 0.66 and 0.70 are derived from the two-dimensional values of the critical exponents $\beta=0.1388$, $v=\frac{4}{3}$, and $\mu=1.298$. As seen in Fig. 5, $\alpha_1(t)$ at $\rho=0.60$ is within 3% of 0.66 from $t=200-3000$. For $R^2(t)$ at $\rho=0.60$, the effective time exponent is essentially constant for t in the range $t=30\,000-70\,000$ with a magnitude approximately 5% greater than 0.70. This small, but marked deviation demonstrates that even for densities within 1.2% of ρ_c, the quantitative behavior of R^2 is already intermediate to the fractal and Euclidean limits. For $t>70\,000$, the gradual increase in $\alpha_2(t)$ signals the incipient crossover to the Euclidean regime. The nonconstant time dependence of R^2 for $t<30\,000$ shows that finite-time effects are significant on this time scale. Therefore, as discussed in Refs. 31 and 35, an accurate scaling description of R^2 for these times requires the inclusion of correction-to-scaling terms which vanish as t goes to infinity.

For densities greater than 0.62, the correlation length is small enough to preclude simultaneously satisfying the inequalities $a^2 \ll R^2(t) \ll \xi^2$. Consequently, the observ-

ables do not exhibit a fractal time dependence, but rather a continuous transition from the short-time behavior to the Euclidean limit. $\alpha_1(t)$ and $\alpha_2(t)$ both illustrate this point: from their initial, intermediate values, they rapidly increase to relatively constant values near 1.0. The density 0.62 is borderline, as seen in Fig. 6. For t up to approximately 5000, $\alpha_2(t)$ is apparently decreasing toward the fractal value; however, at this time it abruptly changes direction and begins a slow crossover to the Euclidean limit.

The departure of $\alpha_1(t)$ and $\alpha_2(t)$ from 1.0 in the long-time limit for densities greater than 0.62 may be attributed to the finite size of the systems we considered. Thus, because $\underline{W}$ is finite dimensional, the density of states for the algebraically smallest eigenvalues, which governs the long-time behavior, is either zero or depleted. The effect of finite size is especially prominent at larger densities since the diffusion coefficient is large, reflecting the high degree of connectivity present in the clusters; the walker thus sees the boundaries at a much earlier time than when on a cluster at a lower density, where the walks are much more convoluted. At $L=800$, the effective time exponent begins to rapidly decrease from its Euclidean value when $R^2(t)\sim 20\,000$–$25\,000$ for the four densities $\rho=0.64$–0.70. Therefore, assuming this decrease is a manifestation of the presence of finite-size effects, the results for $R^2(t)$ and $D(t)$ at $\rho=0.60$ and 0.62 should be valid up to the times shown in Figs. 3, 4, and 6.

Although $\alpha_1(t)$ and $\alpha_2(t)$ are qualitatively similar for densities greater than 0.62, the times for the onset of Euclidean behavior differ dramatically. For example, at $\rho=0.68$, $\alpha_1(t)$ first equals 1.0 at $t\sim 600$, while $\alpha_2(t)\sim 1.0$ at $t\sim 10\,000$. Because $P_0(t)$ depends only on the density of states, whereas $R^2(t)$ depends on both the eigenvalues and eigenvectors of $\underline{W}$, this observation suggests that in spectral space the point at which the eigenvalue distribution becomes similar to that of a regular lattice [$g(\lambda)\sim\lambda^0$ where $g(\lambda)$ is the density of states] is significantly smaller than the point at which the eigenvectors become Euclidean-like (Bloch functions).

The second component of our analysis consisted in verifying the scaling behavior of the diffusion coefficients in the Euclidean regime. According to the arguments presented above, $P_0(t)$ should scale as $[(\rho-\rho_c)^{\mu}t]^{-1}=[D_1(\rho)t]^{-1}$ in the long-time limit, and $R^2(t)$ as $(\rho-\rho_c)^{\mu-\beta}t=D_2(\rho)t$. $D_1(\rho)$ was estimated as $P_0(t)t$ at the time point for which $P_0(t)t$ was "most" Euclidean, that is, the time t such that $|\alpha_1(t)-1.0|$ was a minimum. Similarly, $D_2(\rho)$ was taken to be the value of $\partial R^2(t)/\partial t=D(t,\rho)$ at the time t where $|\alpha_2(t)-1.0|$ was a minimum. These procedures, although plausible, are admittedly *ad hoc* and lacking in rigor. However, in practice, both approaches yielded well-defined and unique time points; moreover, the diffusion coefficients in this time regime were observed (see Fig. 4) to vary by only a few percent over fairly long time intervals, so that any inaccuracy associated with the procedures would most likely be masked by the statistical fluctuations present. This claim is supported by the observation that values of $D_1(\rho)$ and $D_2(\rho)$ obtained by splitting the averages over lattices into two separate sets yielded diffusion coefficients which differed from each other and the full average for the same t by at most a few percent.

Table I lists the estimates of $D_1(\rho)$ at $\rho=0.64$, 0.66, and 0.68 on lattices of length $L=300$ and 500. Table II presents the $D_2(\rho)$ data for $L=300$, 500, and 800. The values of μ and $\mu-\beta$ in Tables I and II, respectively, were obtained by performing a linear least-squares fit through the points $\ln(\rho-\rho_c),\ln D_1(\rho)$ and $\ln(\rho-\rho_c),\ln D_2(\rho)$ and taking μ and $\mu-\beta$ to be the slopes of the resulting lines. The last column in Table II is the sum of the calculated $\mu-\beta$ and the accepted value of $\beta=0.1388$. The estimates of the conductivity exponents shown in Tables I and II are, with the exception of the $L=300$ entry in Table II, in quantitative agreement with the currently accepted value of $\mu=1.296$.[36,57–59] The error in the $L=300$ entry for $D_2(\rho)$ reflects the onset of finite-size effects prior to the times at which $R^2(t)$ has reached the Euclidean regime. This problem does not occur for $P_0(t)$ at $L=300$ since, as discussed above, $P_0(t)$ reaches the Euclidean limit on a much shorter time scale than $R^2(t)$. We should note at this point that we have excluded data at $\rho=0.70$ from Table II on the grounds that at this density, scaling theory is only marginally valid; graphic support for this claim is presented in Fig. 8 below.

In Figs. 7 and 8, the scaling functions $f_1(x)$ and $f_2(x)$ are represented by plotting $P_0(t)(\rho-\rho_c)^{\mu}t$ against $t(\rho-\rho_c)^{2\nu-\beta+\mu}$, and $R^2(t)t^{-d_s/d_F}$ versus $(\rho-\rho_c)^{1/(2\nu-\beta+\mu)}t$. The two graphs reinforce the conclusions previously stated. For densities in the range $\rho=0.62$ to 0.68, the near coincidence of both the $f_1(x)$'s for $x>0.05$ and the $f_2(x)$'s for $1.0<x<2.0$ demonstrate that scaling theory provides an accurate description of transport in the long-time limit. The noticeable shift of $f_2(x)$ at $\rho=0.70$ in the interval $1.0<x<2.0$ indicates scaling arguments are only strictly valid up to $\rho\sim 0.68$. At $\rho=0.60$ and 0.62, $f_2(x)$ appears to be approaching a constant value in the limit as x goes to zero, as expected; the evidence presented here, however, does not conclusively show that scaling theory is quantitatively accurate for these densities in the fractal regime.

In Fig. 9 we plot the relative fluctuations in $R^2(t)$ as a function of time at $L=800$. These graphs were obtained by calculating the standard deviation of $R^2(t)$ from the available data and then normalizing the result by $R^2(t)$. The curves shown are in complete accord with physical intuition. At the smaller densities, the large relative variance in $R^2(t)$ is a direct manifestation of the presence of large spatial fluctuations in the cluster

TABLE I. Euclidean diffusion coefficient $D_1(\rho)$ and conductivity exponent μ for $P_0(t)$.

	$D_1(\rho)$			
L	$\rho=0.64$	$\rho=0.66$	$\rho=0.68$	μ
300	1.4129	0.9077	0.6405	1.289±0.020
500	1.4576	0.9260	0.6528	1.309±0.014

TABLE II. Euclidean diffusion coefficient $D_2(\rho)$ and conductivity exponent μ for $R^2(t)$.

	$D_2(\rho)$				
L	$\rho=0.64$	$\rho=0.66$	$\rho=0.68$	$\mu-\beta$	μ
300	0.4558	0.6520	0.8631	1.04	1.179±0.015
500	0.4233	0.6370	0.8518	1.142	1.283±0.010
800	0.4242	0.6384	0.8710	1.173	1.311±0.008

configurations; at higher densities, the percolating cluster is much more homogeneous. With the exception of $\rho=0.60$ in the time interval [15 000,30 000], the graphs in Fig. 9 are all monotonically decreasing; this again is intuitively obvious, since the observables should at long times lose their memory of the local geometry of the cluster at their initial position.

V. CONCLUSIONS

In the foregoing, we have presented a novel procedure for determining transport observables on random networks. Our results confirm that dynamical scaling theory is quantitative in the Euclidean limit for concentrations up to $\rho=0.68$ and only marginally so for $\rho=0.70$. The calculation of $R^2(t)$ at $\rho=0.60$ is in only qualitative agreement with scaling theory, thereby demonstrating that scaling arguments are strictly valid in the fractal regime only for densities ρ such that $\rho/\rho_c-1<0.012$. Finally, comparisons of $P_0(t)$ and $R^2(t)$ in the long-time limit suggest the distribution of eigenvalues and the eigenvectors of the transfer rate matrix become Euclidean at different points in spectral space.

Because convergence of $R^2(t)$ to the Euclidean limit is relatively slow, many experiments on disordered systems will require time-dependent calculations in the crossover regime. For $\rho>0.60$, this is not rigorously described by a self-similar approximation; instead, the effective time exponent $\alpha_2(t)$ gradually approaches 1. Our numerical calculations produce accurate values of $\alpha_2(t)$ [or, equivalently, of $D(t)$] and thus can be used to interpret such experiments.

The results presented here demonstrate that accurate solution of the master equation via the Lanczos algorithm is computationally feasible, even for very large disordered clusters. We now compare our numerical methods with conventional Monte Carlo simulations.

For a large class of problems, the Lanczos procedure provides qualitatively superior statistics (and hence computational efficiency) as compared to random-walk algorithms. An example of this given here is the calculation of $P_0(t)$, particularly at long times where the infrequency of return to the origin makes collection of accurate statistics prohibitive in alternative approaches. Other

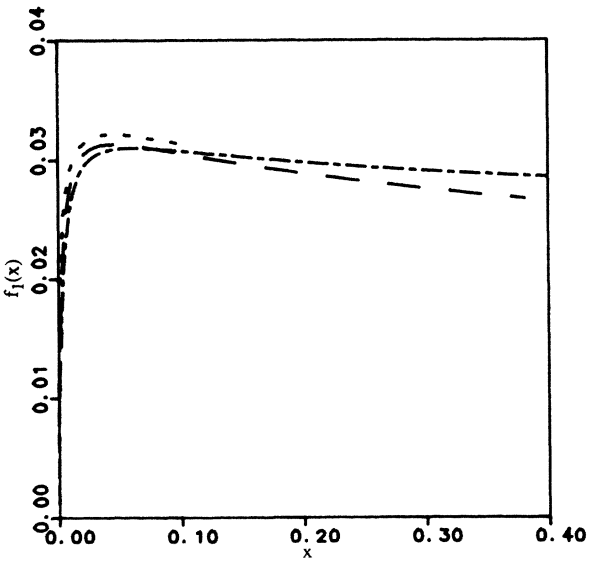

FIG. 7. Graphs of the scaling function $f_1(x)$ where $P_0(t)=[t(\rho-\rho_c)^{\mu}]^{-1}f_1[t(\rho-\rho_c)^{2\nu-\beta+\mu}]$ with ρ_c the percolation threshold, μ the conductivity exponent, ν the correlation length exponent, and β the percolation probability exponent. The graphs were made by plotting $P_0(t)t(\rho-\rho_c)^{\mu}$ vs $t(\rho-\rho_c)^{2\nu-\beta+\mu}$. The three densities shown are $\rho=0.68$ (---), $\rho=0.66$ (— —), and $\rho=0.64$ (---), and are derived from calculations on a lattice of length $L=500$.

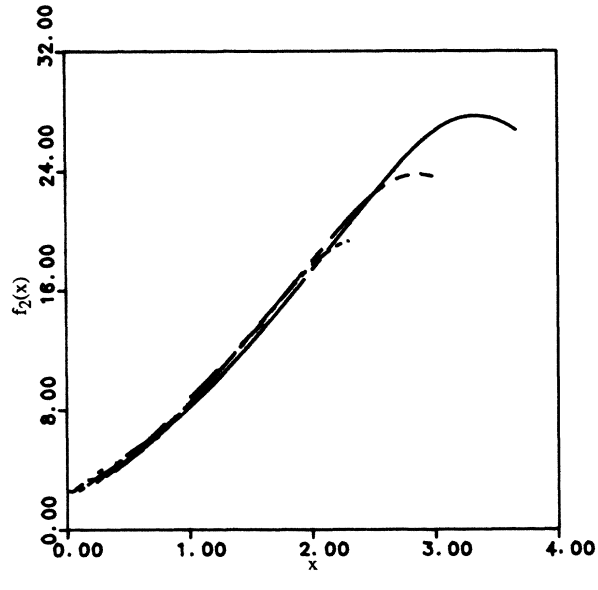

FIG. 8. Plots of the scaling function $f_2(x)$ where $R^2(t)=t^{2\nu/(2\nu-\beta+\mu)}f_2[(\rho-\rho_c)t^{1/(2\nu-\beta+\mu)}]$ with ν the correlation length exponent, β the percolation probability exponent, μ the conductivity exponent, and ρ_c the critical density. The graphs were obtained by plotting $R^2(t)t^{-2\nu/(2\nu-\beta+\mu)}$ against $(\rho-\rho_c)t^{1/(2\nu-\beta+\mu)}$. The six densities shown are $\rho=0.70$ (——-), $\rho=0.68$ (——·——), $\rho=0.66$ (—·—), $\rho=0.64$ (— —), $\rho=0.62$ (---), and $\rho=0.60$ (– – –), and were derived from calculations on a lattice of length $L=800$.

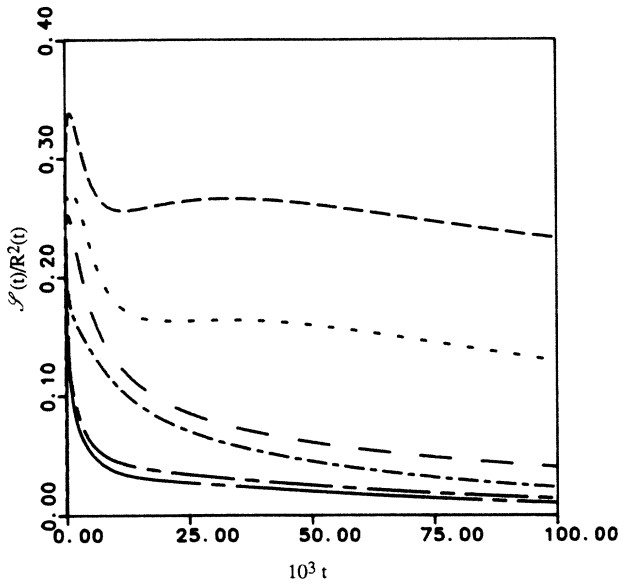

FIG. 9. Graphs depicting the relative fluctuations in $R^2(t)$. The curves were obtained by calculating for each density the standard deviation $\mathcal{S}$ of $R^2(t)$ and then normalizing the result by $R^2(t)[\mathcal{S}(t)/R^2(t)]$. The plots are, from top to bottom, for the densities $\rho=0.60$, 0.62, 0.64, 0.66, 0.68, and 0.70 on lattices of $L=800$. At $\rho=0.60$, 25 cluster configurations were used in determining the standard deviation, and for the remaining densities 15 cluster configurations were available.

such cases, including trapping problems and finite inhomogeneous systems, will be discussed elsewhere.

On the other hand, conventional Monte Carlo methods are well-suited to evaluation of $\langle R^2(t)\rangle$, where every step contributes effectively to the averaging procedure. The principal disadvantage of our approach as currently constituted is the N^2 scaling of computation time as the system size N increases. Consequently, Monte Carlo simulations can utilize much larger systems, thus definitively avoiding finite-size effects. For densities near the percolation edge, this advantage outweighs the automatic averaging over all walks in the Lanczos procedure. While it is difficult to make direct comparisons (due to differences in the specific systems studied and computers employed), we estimate that the Monte Carlo studies of Refs. 31 and 40 require about an order of magnitude less time to achieve a converged set of results for a roughly equivalent large simulation near the percolation threshold.

To overcome this problem, some sort of coarse-graining procedure (which should be accurate at long times) will be required. We are currently pursuing a synthesis of renormalization group techniques with our numerical methods. Because we will still in the end exactly analyze a very large system, the demands on the coarse-graining approximation are much less severe than in methods which utilize the procedure recursively to reduce the problem to a small set of coupled equations. Thus, it should be possible to retain quantitative accuracy while eliminating finite-size effects and reducing the transfer rate matrix dimensionality to an acceptable magnitude.

A final area which we are investigating is the computation of eigenvectors of quantum systems. This work will attempt to directly compute long-time transport properties for disordered quantum systems (e.g., the Anderson Hamiltonian) and to determine the localization properties of the eigenvectors as a function of energy.

ACKNOWLEDGMENTS

This work was supported in part by the Robert A. Welch Foundation and National Science Foundation Materials Research Group Grant No. DMR-8418086. R.A.F. would like to thank the Alfred P. Sloan Foundation and the Camille and Henry Dreyfus Foundation for financial support. We thank Dr. R. E. Wyatt for assistance in the development of the Lanczos code.

[1]R. Kopelman, *Solid State Physics Vol. 4: Spectroscopy and Excitation Dynamics of Condensed Molecular Systems,* edited by V. M. Agranovich and R. M. Hochstrasser (North-Holland, Amsterdam, 1983).
[2]P. Argyrakis and R. Kopelman, Chem. Phys. **78**, 251 (1983).
[3]R. Kopelman, J. Stat. Phys. **42**, 185 (1986).
[4]R. Kopelman, S. Parus, and J. Prasad, Phys. Rev. Lett. **56**, 1742 (1986).
[5]W. D. Dozier, J. M. Drake, and J. Klafter, Phys. Rev. Lett. **56**, 197 (1986).
[6]Y. Song, T. W. Noh, S. Lee, and J. R. Gaines, Phys. Rev. B **33**, 904 (1986).
[7]A. Bunde, W. Dieterich, and E. Roman, Phys. Rev. Lett. **55**, 5 (1985).
[8]T. Odagaki and M. Lax, Phys. Rev. B **24**, 5284 (1981).
[9]G. Korzeniewski, R. A. Friesner, and R. Silbey, J. Stat. Phys. **31**, 451 (1983).
[10]I. Webman, Phys. Rev. Lett. **47**, 1496 (1981).
[11]R. Orbach, J. Stat. Phys. **36**, 735 (1984).
[12]H. Sher and M. Lax, Phys. Rev. B **7**, 4491 (1973).
[13]J. Klafter and R. Silbey, Phys. Rev. Lett. **44**, 55 (1980).
[14]A. A. Kumar and J. Heinrichs, J. Phys. C **13**, 2131 (1980).
[15]R. Fisch and A. B. Harris, Phys. Rev. B **18**, 416 (1978).
[16]R. F. Loring, H. C. Andersen, and M. D. Fayer, J. Chem. Phys. **80**, 5731 (1984).
[17]D. F. Calef, R. A. Friesner, G. Korzeniewski, B. Laird, and R. Silbey, Phys. Rev. A **29**, 2963 (1984).
[18]R. B. Stinchcombe and B. P. Watson, J. Phys. C **9**, 3221 (1976).
[19]J. Machta, J. Stat. Phys. **30**, 305 (1983).
[20]S. Havlin, D. Ben-Avraham, and H. Sompolinsky, Phys. Rev. A **27**, 1730 (1983).
[21]J. Straley, J. Phys. C **13**, 2991 (1980).
[22]S. Alexander and R. Orbach, J. Phys. (Paris) Lett. **43**, L625 (1982).
[23]R. Rammal, J. Stat. Phys. **36**, 547 (1984).

[24]I. Webman, J. Stat. Phys. **36**, 603 (1984).
[25]Y. Gefen, A. Aharony, and S. Alexander, Phys. Rev. Lett. **50**, 77 (1983).
[26]R. Rammal and G. Toulouse, J. Phys. (Paris) Lett. **44**, L13 (1983).
[27]A. Keramiotis, P. Argyrakis, and R. Kopelman, Phys. Rev. B **31**, 4617 (1985).
[28]A. C. Maggs and R. B. Stinchcombe, J. Phys. A **19**, L63 (1986).
[29]R. Biller, J. Phys. A **18**, 989 (1985).
[30]A. Aharony and D. Stauffer, Phys. Rev. Lett. **52**, 2368 (1984).
[31]R. B. Pandey, D. Stauffer, A. Margolina, and J. G. Zabolitzky, J. Stat. Phys. **34**, 427 (1984).
[32]S. Havlin and D. Ben-Avraham, J. Phys. A **16**, L483 (1983).
[33]J. C. Angles d'Auriac and R. Rammal, J. Phys. C **16**, L825 (1983).
[34]P. Argyrakis and R. Kopelman, J. Chem. Phys. **81**, 1015 (1984).
[35]C. Mitescu and J. Roussenq, Ann. Israel Phys. Soc. **5**, 81 (1983).
[36]R. Rammal, J. C. Angles d'Auriac, and A. Benoit, Phys. Rev. B **30**, 4087 (1984).
[37]L. Puech and R. Rammal, J. Phys. C **16**, L1197 (1983).
[38]D. Ben-Avraham and S. Havlin, J. Phys. A **15**, L691 (1982).
[39]S. Wilke *et al.*, J. Phys. A **17**, 647 (1984).
[40]R. B. Pandey and D. Stauffer, Phys. Rev. Lett. **51**, 527 (1983).
[41]R. B. Pandey and D. Stauffer, J. Phys. A **16**, L511 (1983).
[42]A. Nauts and R. E. Wyatt, Phys. Rev. Lett. **51**, 2238 (1983).
[43]G. Zumofen, A. Blumen, and J. Klafter, J. Phys. A **17**, L479 (1984).
[44]G. Zumofen and A. Blumen, Chem. Phys. Lett. **88**, 63 (1982).
[45]A. Blumen, J. Klafter, and G. Zumofen, Phys. Rev. B **28**, 6112 (1983).
[46]R. B. Pandey, Phys. Rev. B **30**, 489 (1984).
[47]E. Seifert and M. Suessenbach, J. Phys. A **17**, L703 (1984).
[48]D. Stauffer, J. Phys. A **18**, 1827 (1985).
[49]R. B. Stinchcombe, J. Phys. A **18**, L591 (1985).
[50]P. Argyrakis and R. Kopelman, Phys. Rev. B **31**, 6008 (1985).
[51]D. Chowdhury and B. K. Chakrabarti, J. Phys. A **18**, L377 (1985).
[52]R. B. Pandey, J. Phys. A **19**, L53 (1986).
[53]C. C. Paige, J. Inst. Math. Appl. **18**, 341 (1972).
[54]C. C. Paige, Linear Algebra Appl. **34**, 235 (1980).
[55]J. Cullum and R. Willoughby, J. Comput. Phys. **44**, 329 (1981).
[56]W. Barth, R. S. Martin, and J. H. Wilkinson, Numer. Math. **9**, 386 (1967).
[57]J. G. Zabolitzky, Phys. Rev. B **30**, 4077 (1984).
[58]D. C. Hong, S. Havlin, H. J. Hermann, and H. E. Stanley, Phys. Rev. B **30**, 4083 (1984).
[59]C. J. Lobb and D. J. Frank, Phys. Rev. B **30**, 4090 (1984).